Biomedicine & Pharmacotherapy 153 (2022) 113487

Contents lists available at ScienceDirect

Biomedicine & Pharmacotherapy

journal homepage: www.elsevier.com/locate/biopha

Pimitespib, an HSP90 inhibitor, augments nifuroxazide-induced disruption in the IL-6/STAT3/HIF-1α autocrine loop in rats with bleomycin-challenged lungs: Evolutionary perspective in managing pulmonary fibrosis

Dalia H. El-Kashef [a], Mahmoud E. Youssef [b], Mohamed Nasr [c,d], Mohammed Alrouji [e,*], Sharif Alhajlah [e], Othman AlOmeir [f], Noura El Adle Khalaf [g], Dalia M. Abdel Ghaffar [h], Lubna Jamil [i], Zeinab M. Abdel-Nasser [j], Samar Ibrahim [k], Mahmoud Said Ibrahim Abdeldaiem [l,m], Sally S. Donia [n], Osama A. Mohammed [o,p], Nesreen Elsayed Morsy [q], Ahmed Shata [r,s], Sameh Saber [b,*]

[a] Department of Pharmacology and Toxicology, Faculty of Pharmacy, Mansoura University, Mansoura 35516, Egypt
[b] Department of Pharmacology, Faculty of Pharmacy, Delta University for Science and Technology, Gamasa 11152, Egypt
[c] Department of Pharmaceutics and Industrial Pharmacy, Faculty of Pharmacy, Helwan University, Cairo 11790, Egypt
[d] Department of Pharmaceutics, Faculty of Pharmacy, Delta University for Science and Technology, Gamasa 11152, Egypt
[e] Department of Medical Laboratories, College of Applied Medical Sciences, Shaqra University, Shaqra 11961, Saudi Arabia
[f] Department of Pharmacy Practice, College of Pharmacy, Shaqra University, Shaqra 11961, Saudi Arabia
[g] Department of Clinical Pharmacology, Faculty of Medicine, Mansoura University, Mansoura 35516, Egypt
[h] Department of Physiology, Faculty of Medicine, Mansoura University, Mansoura 35516, Egypt
[i] Department of Histology, Faculty of Medicine, October 6 University, Giza 12511, Egypt
[j] Department of Biochemistry, Faculty of Pharmacy, October University for Modern Sciences and Arts (MSA), Giza 11787, Egypt
[k] Department of Pharmacy Practice, Faculty of Pharmacy, Ahram Canadian University, Giza, Egypt
[l] Clinical Pharmacy Discipline, School of pharmaceutical sciences, Universiti Sains Malaysia, Penang, Malaysia
[m] Pharmacy Practice Department, Faculty of Pharmacy, Sinai University, Ismailia, Egypt
[n] Department of Clinical Physiology, Faculty of Medicine, Menoufia University, Menoufia, Egypt
[o] Department of Clinical Pharmacology, Faculty of Medicine, Ain Shams University, Cairo 11566, Egypt
[p] Department of Clinical Pharmacology, Faculty of Medicine, Bisha University, Bisha 61922, Saudi Arabia
[q] Pulmonary medicine Department, Mansoura university sleep center, Faculty of Medicine, Mansoura University, Mansoura 35516, Egypt
[r] Department of Clinical Pharmacology, Faculty of Medicine, Mansoura University, Mansoura 35516, Egypt
[s] Department of Clinical Pharmacy, Faculty of Pharmacy, Delta University for Science and Technology, Gamasa 11152, Egypt

ARTICLE INFO

Keywords:
Bleomycin
Nifuroxazide
Pimitespib
STAT3

ABSTRACT

Idiopathic pulmonary fibrosis is a fatal lung disorder in which the etiology and pathogenesis are still unobvious. Effective treatments are urgently needed considering that lung transplantation is the only treatment that could improve outcomes. This study aimed to investigate the therapeutic significance of the dual administration of pimitespib, an HSP90 inhibitor, and nifuroxazide, a STAT3 inhibitor, against bleomycin-induced pulmonary

Abbreviations: BALF, bronchoalveolar lavage fluid; CREB, cAMP response element-binding protein; ECM, extracellular matrix; EE, entrapment efficiency; HIF-1α, hypoxia-inducible factor-1α; HSP90, heat shock protein 90; IL-6, interleukin-6; IPF, idiopathic pulmonary fibrosis; LDH, lactate dehydrogenase; MMP-1, matrix metalloproteinase-1; mTOR, mammalian target of rapamycin; NOx, total nitrite and nitrate; NFX, nifuroxazide; p300 HAT, histone acetyltransferase p300; PDGF-BB, platelet derived growth factor-BB; PIMI, pimitespib; STAT3, signal transducer and activator of transcription 3; TGF-β, transforming growth factor-β; TIMP-1, tissue inhibitor of metalloproteinase-1; TNF-α, tumor necrosis factor-α.

* Corresponding authors.
E-mail addresses: dalia_elkashef@mans.edu.eg (D.H. El-Kashef), mahmoodelsaid@hotmail.com (M.E. Youssef), m2nasr@yahoo.com (M. Nasr), malrouji@su.edu.sa (M. Alrouji), alhjlah@su.edu.sa (S. Alhajlah), aalomear@su.edu.sa (O. AlOmeir), nouraeladle@mans.edu.eg, nonnos_86@hotmail.com (N. El Adle Khalaf), Dalia.mr@mans.edu.eg (D.M.A. Ghaffar), drlubnajamil1978@gmail.com (L. Jamil), zmohamed@msa.edu.eg (Z.M. Abdel-Nasser), samaribrahim370@gmail.com (S. Ibrahim), mahmoud.said@su.edu.eg (M.S.I. Abdeldaiem), sallydonia@yahoo.com (S.S. Donia), osamaabbass@med.asu.edu.eg, oamohamed@ub.edu.sa, drosamaabbass@gmail.com (O.A. Mohammed), neselmorsy@mans.edu.eg (N.E. Morsy), ahmedmhes@mans.edu.eg (A. Shata), sampharm81@gmail.com (S. Saber).

https://doi.org/10.1016/j.biopha.2022.113487
Received 17 June 2022; Received in revised form 15 July 2022; Accepted 27 July 2022
Available online 31 July 2022

HIF-1α
IL-6/STAT3/HIF-1α autocrine loop

fibrosis in rats. Our results revealed that pimitespib/nifuroxazide inhibited bleomycin-induced alterations in the structure and the function of the lungs. They demonstrated significant decreases in the BALF total and differential cell counts, LDH activity, and total protein. Concurrently, there was a reduction in the accumulation of collagen as proved by decreased hydroxyproline and the gene expression of COL1A1 accompanied by lower levels of PDGF-BB, TIMP-1, and TGF-β. The levels of IL-6 were also downregulated. Pimitespib-induced inhibition of HSP90 led to subsequent inhibition of HIF-1α and STAT3 client proteins since the closed HSP90 would not enclose its client proteins. Therefore, pimitespib resulted in the repression of HIF-1α/CREB-p300 HAT as well as the STAT3/CREB-p300 HAT nuclear interactions. On the other hand, nifuroxazide resulted in a notable decline in pSTAT3 and HIF-1α levels. Subsequently, the combined effects of both drugs led to a substantial reduction in ECM deposition. Herein, pimitespib augmented nifuroxazide-induced disruption in the IL-6/STAT3/HIF-1α autocrine loop. Our findings also disclose that this novel loop is a promising therapeutic attack site for possible pulmonary fibrosis repression studies. Therefore, the use of pimitespib/nifuroxazide embodies an evolutionary perspective in managing pulmonary fibrosis.

1. Introduction

Pulmonary fibrosis (PF) is a progressive fatal lung disease associated with difficulty in respiration, disrupted lung functions [1,2], irreversible respiratory failure, and ultimately death [3]. Idiopathic pulmonary fibrosis (IPF), a severe form of PF with unknown etiology, has a life expectancy of 2–6 years after diagnosis [4]. IPF is characterized by deterioration of the alveolar structure, increased fibroblast proliferation, and increased deposition of extracellular matrix (ECM) [5]. Age, male sex, and comorbidities such as diabetes and hypertension are among the risk factors for IPF. Besides, patients with IPF who are debilitated by lowered pulmonary reserve are believed to be more susceptible to infection with COVID-19 than the general population [6]. Despite extensive efforts, the etiology and pathogenesis of the disease are still unobvious. Lung transplantation is the only treatment that could improve outcomes. Owing to many challenges that could face transplantation, effective treatments with minimal side effects are urgently needed [7].

Bleomycin-induced PF is a well-established animal model that is widely used due to its reproducibility and ability to reflect many features of IPF [8]. It has been documented that the production of pro-inflammatory cytokines comprising tumor necrosis factor-α (TNF-α), interleukin-6 (IL-6), transforming growth factor-β (TGF-β), and oxidative stress are implicated in the pathogenesis of bleomycin-induced PF [9]. IL-6 prompts the activation of Janus kinases and finally signal transducer and activator of transcription 3 (STAT3), which is a dormant cytoplasmic transcription factor. Additionally, IL-6 provokes several responses, both pro-inflammatory and pro-fibrotic, based upon the pathological condition [10,11]. Earlier studies reported that IL-6 is elevated in mouse models of bleomycin-induced PF [12] and lungs of patients with IPF [13]. Thus, targeting IL-6 and the subsequent inhibition of STAT3 could offer an alternative therapy to PF. Nifuroxazide (NFX) is an oral nitrofuran broad-spectrum antibacterial. It is commonly used as an intestinal disinfectant for the treatment of infectious diarrhea or colitis [14]. Nifuroxazide has been described as a STAT3 inhibitor, which prompts the expression of multiple genes, comprising pro-inflammatory genes [15]. Moreover, a recent study reported that nifuroxazide ameliorates PF by blocking myofibroblast genesis and STAT3 activation [16]. Saber, et al. [17] clearly described the importance of cubosomes as a drug delivery system in enhancing the bioavailability of nifuroxazide where they showed that the mean relative bioavailability of cubosomal dispersion was two-fold higher in terms of AUC 0-α. Additionally, they showed that nifuroxazide-loaded cubosomal dispersion significantly affects nifuroxazide concentration and distribution in lung tissues compared to nifuroxazide suspension.

Hypoxia is a hallmark aspect of chronic tissue injury and fibrosis. Mechanisms beyond hypoxia include inadequate blood supply, this is attributed to vascular damage and incursion of high-oxygen-consuming inflammatory cells. The microenvironmental nature of tissue hypoxia induces the hypoxia-inducible factor-1α (HIF-1α), the main transcription factor controlling oxygen homeostasis [18,19]. It was anticipated that heat shock protein 90 (HSP90) is a major regulator in HIF-1 activation because HIF-1 activity is inhibited in the presence of geldanamycin which is an HSP90 inhibitor. Pimitespib (PIMI) belongs to a novel class of orally active selective inhibitors of HSP90α and β [20], which revealed antitumor activity in a human non-small cell lung cancer xenograft rat model without detectable ocular toxicities [21], and demonstrated efficacy in preclinical models of adult T-cell leukemia [22]. Indeed, other HSP90 inhibitors have been recently studied against PF. It was proven that AUY-922 inhibits the development of nitrogen mustard-induced PF by modifying the levels of profibrotic proteins, reducing the expression and deposition of collagen and preserving the lung dynamics [23]. Moreover, the HSP90 Inhibitor, AT13387, protected the alveolo-capillary barrier and prevented HCl-induced chronic lung injury and pulmonary fibrosis [24].

This study aimed to investigate the therapeutic significance of the dual administration of pimitespib and nifuroxazide against bleomycin-induced PF with a particular emphasis on the STAT3/HIF-1α interplay. Herein, we propose that pimitespib, as adjunctive therapy, may augment the antifibrotic effects of the STAT3 inhibitor nifuroxazide by disrupting both the nuclear translocation of pSTAT3 and HIF-1α and their interactions with histone acetyltransferase p300 (p300 HAT)/cAMP response element-binding protein (CREB) co-activators. p300 HAT and CREB are two closely related transcriptional co-activating proteins with similar structures. They interact with numerous transcription factors and act to increase the expression of their target genes. Additionally, p300 HAT and CREB are involved in the IL-6/STAT3 signaling [25,26]. Additionally, these genes have also been identified as co-activators of HIF-1α [27,28] and thus, play a role in the stimulation of hypoxia-inducible genes. In this study, nifuroxazide was prepared as a cubosomal dispersion to maximize the bioavailability and lung delivery of the drug as previously described [17].

2. Materials and methods

2.1. Materials

All materials, drugs, and assay kits and suppliers are described as follows: bleomycin (bleocel®, 15 mg/vial) was supplied by Cell Pharm GmbH (Bad Vilbel, Germany); nifuroxazide was supplied by Amoun Pharmaceutical Company (Cairo, Egypt); pimitespib from Active Biochem (China); phosphate-buffered saline, total nitrite/nitrate assay kit, hydroxyproline assay kit, histone acetyltransferase activity (HAT) assay kit, and LDH activity assay kit were provided by Sigma-Aldrich (St. Louis, MO, USA); poloxamer 407 (p407) was obtained from Sigma-Aldrich (Milwaukee, WI, USA); neutral-buffered formalin was obtained from El-Gomhouria Co (Cairo, Egypt); RNAlater, Rneasy mini kit, and reverse transcriptase were obtained from Qiagen (Germany); SYBR green PCR master mix from Qiagen (USA); total protein content assay kit was supplied by Spinreact, S.A./S.A.U. (Santa Coloma, Spain); platelet derived growth factor-BB (PDGF-BB) assay kit, BCA protein assay kit, nuclear extraction assay kit, and Bradford reagent were obtained from

Abcam (Cambridge, UK); tissue inhibitor of metalloproteinase-1 (TIMP-1) and IL-6 assay kit were provided by R&D systems (Minneapolis, MN, USA); transforming growth factor beta (TGF-β) and heat shock protein 70 (HSP70) assay kits were supplied by MyBioSource Inc. (San Diego, CA, USA); hypoxia-inducible factor-1α (HIF-1α) assay kit and tissue lysis buffer were provided by Thermo Fisher Scientific Inc. (Rockford, USA); TransAM pCREB transcription factor assay kit from Active Motif; phospho-STAT3 (Tyr705) assay kit was supplied by RayBiotech (Norcross, GA, USA); phospho-mTOR (S2448) assay kit was obtained from Cell Signaling Technology (Massachusetts, USA); glyceryl monooleate (GMO) from Gattefosse (France); formic acid, ammonium format, acetic acid, ammonium acetate, acetonitrile, and methanol were obtained from Fisher Scientific (Waltham, MA, USA).

2.2. Preparation of nifuroxazide-loaded cubosomal nanoparticles

Nifuroxazide-loaded cubosomal dispersions were prepared as described previously [17]. The TEM (model JEM-2100, JEOL, Japan) was used to observe the nanoparticles. A Zetasizer Nano ZS (Malvern Instruments, UK) was used for the particle size and zeta potential measurements. After separation of the unentrapped nifuroxazide, A validated LC-MS/MS method was used to analyze the obtained supernatant, and the entrapment efficiency (EE percent) was calculated using the equation: EE (%) = (total nifuroxazide - unentrapped nifuroxazide)/total nifuroxazide.

2.3. Experimental study and treatment protocol

2.3.1. Animals

Male Sprague Dawley rats (6–8-week-old) weighing 210 ± 15 g purchased from Theodor Bilharz Research Institute were permitted to acclimatize for one week before beginning experiments. The protocols followed the guidelines of the Delta University for Science and Technology's Institutional Animal Care and Use Committee; approval number (FPDU3520/4).

2.3.2. Pulmonary fibrosis rat model

Intraperitoneal injection (i.p.) of sodium thiopental (20 mg/kg) was used to anesthetize the animals to make a midline neck incision with the aid of a surgical blade. Then, using a 26-gauge needle, bleomycin (5 mg/kg) in saline was deliberately infused into the exposed trachea followed by repeated twisting of rats' bodies while maintained at a reverse Trendelenburg position to ensure that the solution is distributed uniformly throughout the lung tissue. As an antiseptic, a povidone-iodine solution was applied to the sutured area.

2.3.3. Experimental design

Animals were randomly assigned to 7 groups as follows: 1) **Normal** group; 2) **PIMI** group, rats received pimitespib (10 mg/kg/day; p.o./four weeks); 3) **NFX-cub** group, rats received NFX-cub (20 mg/kg/day; p.o./four weeks); 4) **BLEO** group, rats received intratracheal instillation of Bleomycin (5 mg/kg); 5) **BLEO/PIMI** group, rats received intratracheal instillation of Bleomycin and pimitespib (10 mg/kg/day; p.o./four weeks); 6) **BLEO/NFX-cub** group, rats received intratracheal instillation of Bleomycin and NFX-cub (20 mg/kg/day; p.o./four weeks); 7) **BLEO/PIMI/NFX-cub** group, rats received intratracheal instillation of Bleomycin, pimitespib, and NFX-cub. The same anesthesia protocol was used on all rats. A sham surgical operation and the intratracheal instillation of saline were used on control rats. Bleomycin was intratracheally instilled for once on the first day of the experiment. At the end of the experimental protocol, rats were euthanized with secobarbital (50 mg/kg; i.p.) **(**Table 1**)**.

Table 1
Experimental design.

Exp. groups	Day 1	Day 2–28
Normal **(n = 8)**	Anesthetization protocol Sham operation Intratracheal instillation of saline	–
PIMI **(n = 8)**	Anesthetization protocol Sham operation Intratracheal instillation of saline Pimitespib (10 mg/kg, p.o.)	Pimitespib (10 mg/kg, p.o.)
NFX-cub **(n = 8)**	Anesthetization protocol Sham operation Intratracheal instillation of saline nifuroxazide-loaded cubosomes (20 mg/kg; p.o.)	nifuroxazide-loaded cubosomes (20 mg/kg; p.o.)
BLEO **(n = 10)**	Anesthetization protocol Surgical procedure intratracheal instillation of bleomycin (5 mg/kg)	–
BLEO/PIMI **(n = 8)**	Anesthetization protocol Surgical procedure intratracheal instillation of bleomycin (5 mg/kg) Pimitespib (10 mg/kg, p.o.)	Pimitespib (10 mg/kg, p.o.)
BLEO/NFX-cub **(n = 8)**	Anesthetization protocol Surgical procedure Intratracheal instillation of bleomycin (5 mg/kg) Nifuroxazide-loaded cubosomes (20 mg/kg; p.o.)	nifuroxazide-loaded cubosomes (20 mg/kg; p.o.)
BLEO/PIMI/NFX-cub **(n = 8)**	Anesthetization protocol Surgical procedure Intratracheal instillation of bleomycin (5 mg/kg) Pimitespib (10 mg/kg, p.o.) Nifuroxazide-loaded cubosomes (20 mg/kg; p.o.)	Pimitespib (10 mg/kg, p.o.) Nifuroxazide-loaded cubosomes (20 mg/kg; p.o.)

2.4. Collection of bronchoalveolar lavage fluid (BALF) and lung tissue

The BALF was collected (75% yield) as described by Saber, et al. [17] followed by centrifugation for 10 min at 2000 rpm/4 °C. The total and differential cell counts were determined in the pellets after being separated. Smeared preparation stained with Giemsa stain was used for 200 cells and employed for cell differentiation. After being excised, lung tissues were rinsed with PBS and the left lungs were kept for 24 h in formalin (4%). Other parts of the right lungs were kept in RNAlater or preserved at − 80 °C.

2.5. Histological examination

The left lungs were processed and fixed in paraffin before being cut into 4-μm sections. The staining procedures used were standard hematoxylin and eosin (H&E) or Masson's trichrome [29,30]. The following scores were used to assess the inflammatory-cell infiltration: 0, absence of inflammation; 1, very mild; 2, mild; 3, moderate; 4, severe; and 5, an extreme degree of inflammation. Standardized quantification method of pulmonary fibrosis in histological samples is used to evaluate the degree of fibrotic changes in bleomycin-challenged lung tissues as previously described [31]. Table 2 describes the characterization of the grading system.

2.6. Determination of BALF total protein content, lactate dehydrogenase (LDH) activity, total nitrite/nitrate content (NOx), and hydroxyproline in lung tissue

BALF total protein content was determined in duplicate by using copper salts in an alkaline medium to form an intense violet-blue complex with proteins and measuring absorbance at 546 nm. BALF LDH activity was evaluated using the reduction of NAD to NADH, which was measured at 450 nm. Total NO metabolite levels were determined using

Table 2
Grading characterization of the fibrotic tissue changes.

Fibrosis grade	Microscopic structure	Characteristic features
0	Alveolar septa	No fibrotic depositions not more that insubstantial small fibers in some alveolar walls
	Lung structure	Normal lung
1	Alveolar septa	Isolated mild fibrotic changes
	Lung structure	Alveoli partly enlarged and rarefied, but no fibrotic masses
2	Alveolar septa	Visibly fibrotic changes (septa >3 × thicker than normal) with knot-like formation but not linked to each other
	Lung structure	Partly enlarged alveoli and rarefied, but no fibrotic masses
3	Alveolar septa	Fibrotic walls are contiguous (septa >3 × thicker than normal) mostly in whole the field
	Lung structure	Alveoli partly enlarged and rarefied, but no fibrotic masses
4	Alveolar septa	Variable
	Lung structure	Single fibrotic masses (≤ 10% of the field)
5	Alveolar septa	Variable
	Lung structure	Fibrotic masses are confluent (>10% and ≤ 50% of the field). Lung structure cruelly damaged but still conserved
6	Alveolar septa	Variable, mostly not existent
	Lung structure	Large contiguous fibrotic masses (> 50% of the field). Lung architecture mostly not conserved
7	Alveolar septa	Non-existent
	Lung structure	Alveoli nearly obliterated with fibrous masses but still up to five air bubbles
8	Alveolar septa	Non-existent
	Lung structure	Complete obliteration with fibrotic masses in the field

the nitrite/nitrate assay. Hydroxyproline is a well-known collagen content estimator. The reaction of oxidized hydroxyproline with 4-(dimethylamino) benzaldehyde yielded the colored product, which was measured at 560 nm.

2.7. ELISA measurements

According to the corresponding manufacturer's instructions, the levels of platelet-derived growth factor-BB (PDGF-BB), tissue inhibitor of metalloproteinase-1 (TIMP-1), IL-6, TGF-β, and heat shock protein 70 (HSP70) were determined. HSP70 was determined as a surrogate marker of HSP90 inhibition. Hypoxia-inducible factor-1α (HIF-1α) was measured as described by Saber, et al. [17].

2.8. Determination of p300 HAT and CREB activity

In brief, 100 mg of lung tissue was cut into small pieces and placed in a homogenizer, followed by 0.5 ml of pre-extraction buffer containing DTT Solution. The mixture was then incubated on ice for 15 min before being centrifuged for 10 min at 12,000 rpm at 4 °C and the supernatant was removed. The nuclear pellet was treated with an extraction buffer containing DTT and a protease inhibitor cocktail. Incubated on ice for 15 min, with a 5-second vortex every 3 min. The extract was then sonicated three times for ten seconds. The suspension was centrifuged for 10 min at 14,000 rpm at 4 °C before being transferred to a new microcentrifuge vial. The nuclear extract's protein concentration was determined using the Bradford reagent. Based on the fact that acetylation of a peptide substrate by active HAT releases the free form of CoA, which serves as an essential coenzyme for NADH production, HAT activity was determined in the nuclear extract. When NADH reacts with a soluble tetrazolium dye, it can be detected spectrophotometrically. The normalized relative O.D. value per g nuclear protein was used to express HAT activity. Cyclic AMP response element-binding protein (CREB) activity was also measured in nuclear extracts. A cyclic AMP response element (5'-TGACGTCA-3') immobilized on a 96-well plate binds to the nuclear extract's CREB. Then, a primary antibody recognizes p-CREB at Ser133. A colorimetric readout is provided by a secondary HRP-conjugated antibody. The relative O.D. value per g nuclear protein was used to express CREB activity.

2.9. Determination of the STAT3 and mTOR

For 0.1 g of lung tissue, 1 ml of lysis buffer was used to homogenize it. Following this, the tissue lysate is sonicated. The buffer was composed of 20 mM Tris-HCl (pH 7.5), 150 mM NaCl, 1 mM Na2EDTA, 1 mM EGTA, 1% Triton, 2.5 mM sodium pyrophosphate, 1 mM beta-glycerophosphate, 1 mM Na3VO4, and 1 g/ml leupeptin in the presence of a protease inhibitor cocktail and phosphatase inhibitor. The BCA protein assay was used to determine the sample protein concentration in the extract, and samples were diluted to the desired concentration using the buffer before being stored at − 80 °C. pSTAT3 (Tyr705) optical density values were determined and those of the STAT3 pan protein were measured in the remaining wells and used to normalize the data. The previous method for preparing tissue lysate was used to determine the pmTOR. The microwells have been coated with an mTOR mouse antibody. The coated antibody captures mTOR (phosphorylated and non-phosphorylated) protein after incubation with lysates. To detect the captured pmTOR protein, a pmTOR (S2448) rabbit antibody was added after extensive washing. The bound detection antibody was then recognized using an anti-rabbit IgG, HRP-linked antibody. TMB is added to the HRP substrate to develop color. The magnitude of this developed color's absorbance is proportional to the amount of mTOR phosphorylated at S2448. The results were presented as normalized optical density values. It is to be noted that decreased mTOR activity upregulates the removal of dysfunctional cellular components via autophagy [32,33].

2.10. qRT-PCR for the expression of TGF-β1, Collagen type I, alpha 1 (COL1A1), and STAT3 in lung tissue

RNA was extracted and the total amount and purity were determined using NanoDrop. RNA was reverse transcribed and the PCR reaction was performed in triplicate using thermocycler Rotor-Gene Q and using SYBR Green PCR Master Mix. Relative expression was calculated using the comparative cycle threshold (Ct) ($2^{-\Delta\Delta CT}$) method. The sequences of PCR primer pairs for TGF-β1, F: 5'-CTTCTCCACCAACTACTGCTTC-3′and R: 5'-GGGTCCCAGGCAGAAGTT-3′; Collagen type I, alpha 1 (COL1A1), F: 5'-GACATGTTCAGCTTTGTGGACCC-3′and R: 5'-AGGGACCCTTAGGCCATTGTGTA-3′; STAT3, F: 5'-AGAGGCGGCAGCAGATAGC-3′and R: 5'-TTGTTGGCGGGTCTGAAGTT-3′; and GAPDH, F: 5'-TCAAGAAGGTGGTGAAGCAG-3′and R: 5'-AGGTGGAAGAATGGGAGTTG-3′. All values were normalized to the GAPDH gene. Rotor-Gene Q Software 2.1 (Qiagen) was used for data analysis.

2.11. Statistical analysis

To conduct statistical analysis, GraphPad Prism software version 6 (GraphPad Software Inc., La Jolla, CA, USA) was used. The data are presented as the mean ± standard deviation (SD). A one-way analysis of variance was used to examine group differences, followed by a Tukey's Kramer post hoc multiple comparisons test. For non-parametric data, the Kruskal–Wallis test and Dunn's post hoc test were used to assess differences between groups (inflammation and fibrotic scores). P values less than 0.05 were deemed statistically significant.

3. Results

3.1. The particle morphology, particle size, and EE % of the nifuroxazide cubosomes

Based on our recent work [17], the polyangular-shaped

nanoparticles exhibited a mean particle size and zeta potential of 223.73 ± 4.73 nm and − 20.93 ± 2.38 mV, respectively. The EE was 90.56 ± 4.25%.

3.2. Effect of pimitespib, nifuroxazide and their combined therapy on total leukocyte, lymphocyte, and neutrophil counts in the BALF

Intra-tracheal instillation of bleomycin resulted in a significant elevation in total and differential cell counts when compared to the normal group. Oral administration of either PIMI, NFX-cub, and in particular their combination with bleomycin-challenged rats significantly decreased these elevated levels upon comparison with the BLEO group **(**Fig. 1**)**.

3.3. Effect of pimitespib, nifuroxazide and their combined therapy on NOx, LDH, and total protein levels in the BALF

BLEO group exhibited a substantial increase in the levels of NOx **(**Fig. 2**A)**, LDH **(**Fig. 2**B),** and total protein **(**Fig. 2**C)** in the BALF relative to the normal group. Co-treatment of either PIMI and NFX-cub and in particular their combination with bleomycin significantly reduced levels of NOx, LDH, and total protein when compared to the BLEO group.

3.4. Effect of pimitespib, nifuroxazide and their combined therapy on hydroxyproline and the mRNA expression of COL1A1 in lung tissues

Instillation of bleomycin produced a substantial increase in hydroxyproline content **(**Fig. 3**A)** and the mRNA expression of Col1A1 **(Figure3B)** when compared to the normal group. BLEO/PIMI, BLEO/NFX-cub, and in particular the BLEO/PIMI/NFX-cub group of rats revealed a marked decrease in hydroxyproline content and the mRNA expression of Col1A1 upon comparison with the BLEO group.

3.5. Effect of pimitespib, nifuroxazide and their combined therapy on the levels of PDGF-BB, TIMP-1, and TGF-β in lung tissues

Fig. 4 showed that intra-tracheal instillation of bleomycin-induced a profound elevation in the levels of PDGF-BB **(**Fig. 4**A)**, TIMP-1 **(**Fig. 4**B),** and TGF-β **(**Fig. 4**C)** as well as the mRNA expression of TGF-β **(**Fig. 4**D)** in relative to the normal group. Oral treatment with PIMI and NFX-cub and their combination significantly reversed these elevated levels when compared to the BLEO group. Tissue levels of all these markers, except TGF-β mRNA, were significantly declined after combined treatment with PIMI and NFX-cub compared with their individual administration.

3.6. Effect of pimitespib, nifuroxazide, and their combined therapy on HSP70 levels in lung tissues

HSP70 is considered a surrogate marker of HSP90 inhibition. As shown in Fig. 5, bleomycin instillation produced a significant increase in the levels of HSP70 when compared to the normal group ($p < 0.05$). PIMI, NFX-cub, and in particular the PIMI/NFX-cub group increased HSP70 to levels with significant differences from both the normal and BLEO groups. Reported HSP70 elevation after administration of PIMI/NFX-cub combination to bleomycin-insulted rats was significantly increased compared with the BLEO/PIMI group. In this regard, NFX-cub seems to potentiate the HSP90 inhibiting activity of Pimitespib.

3.7. Effect of pimitespib, nifuroxazide and their combined therapy on the levels of IL-6, HIF-1α, p300 HAT, and CREB in lung tissues

Fig. 6 shows that bleomycin resulted in a significant increase in the levels of IL-6 **(**Fig. 6**A)**, HIF-1α **(**Fig. 6**B)**, p300 HAT **(**Fig. 6**C),** and CREB **(**Fig. 6**D)** when compared to the normal group. Daily oral administration of PIMI, NFX-cub, and their combination significantly reduced these elevated levels. However, the BLEO/NFX-cub group failed to produce a significant difference in the level of CREB activity when compared to the BLEO group.

3.8. Effect of pimitespib, nifuroxazide and their combined therapy on the mRNA expression of STAT3 and the levels of p-STAT3 in lung tissues

Intra-tracheal instillation of bleomycin produced a marked elevation in the mRNA expression of STAT3, and the levels of normalized p-STAT3 when compared to the normal group. BLEO/NFX-cub and BLEO/PIMI/NFX-cub groups showed a significant decrease in these parameters when compared to the BLEO group. Pimitespib in the BLEO/PIMI group failed to affect the mRNA expression of STAT3 and the levels of normalized p-STAT3 when compared to the BLEO group (Fig. 7**)**.

3.9. Effect of pimitespib, nifuroxazide, and their combined therapy on p-mTOR in lung tissues

Fig. 8 showed that the instillation of bleomycin significantly

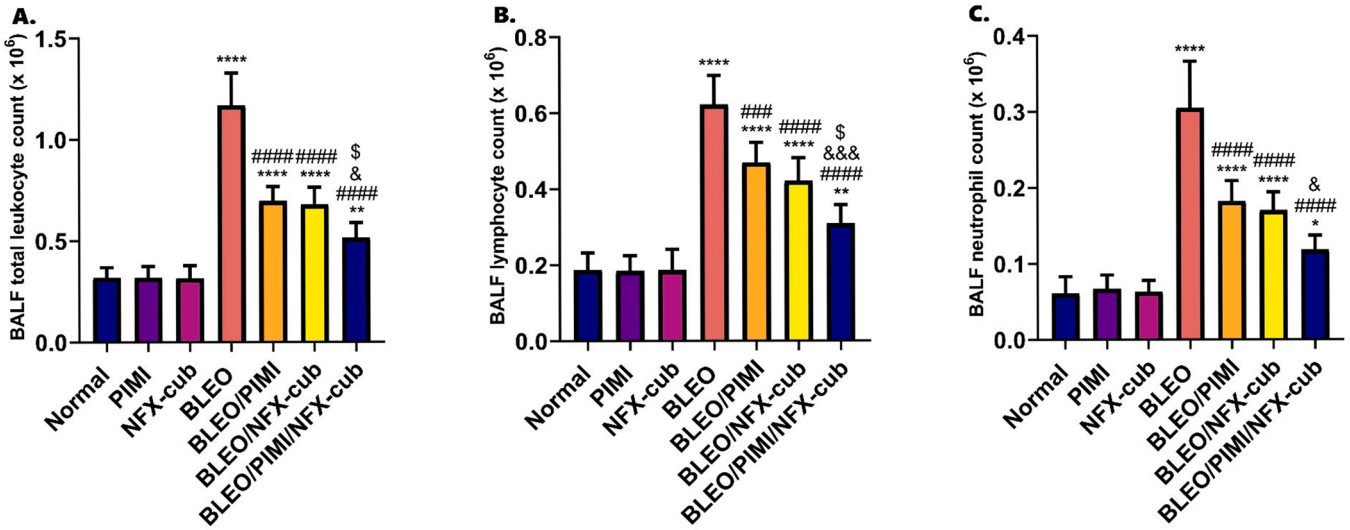

Fig. 1. Effect of pimitespib, nifuroxazide, and their combined therapy on total leukocyte count (A); lymphocyte count (B); and neutrophil count (C) in the BALF. $P \leq 0.05$ indicates a statistical significance. * , vs Normal; #, vs BLEO; &, vs BLEO/PIMI; $, vs BLEO/NFX-cub. Levels of significance were used as follows: one symbol, $P \leq 0.05$; two symbols, $P \leq 0.01$; three symbols, $P \leq 0.001$; four symbols, $P \leq 0.0001$.

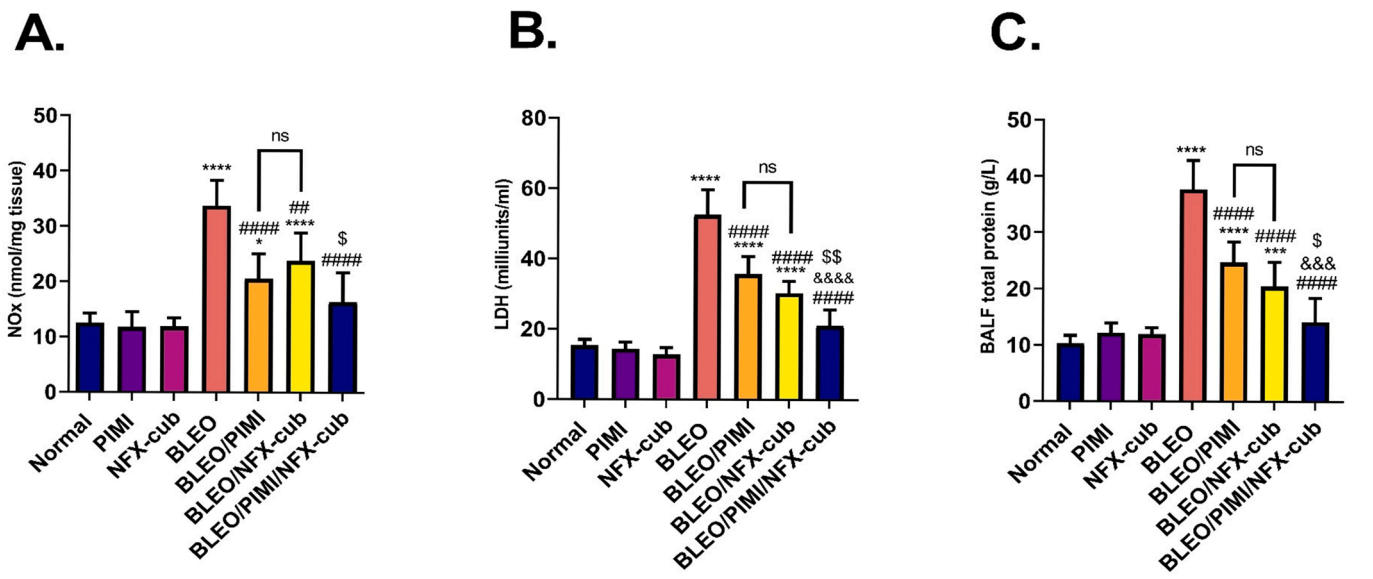

Fig. 2. Effect of pimitespib, nifuroxazide, and their combined therapy on NOx (A), LDH (B) and total protein (C) levels in the BALF. $P \leq 0.05$ indicates a statistical significance. * , vs Normal; #, vs BLEO; &, vs BLEO/PIMI; $, vs BLEO/NFX-cub. Levels of significance were used as follows: one symbol, $P \leq 0.05$; two symbols, $P \leq 0.01$; three symbols, $P \leq 0.001$; four symbols, $P \leq 0.0001$.

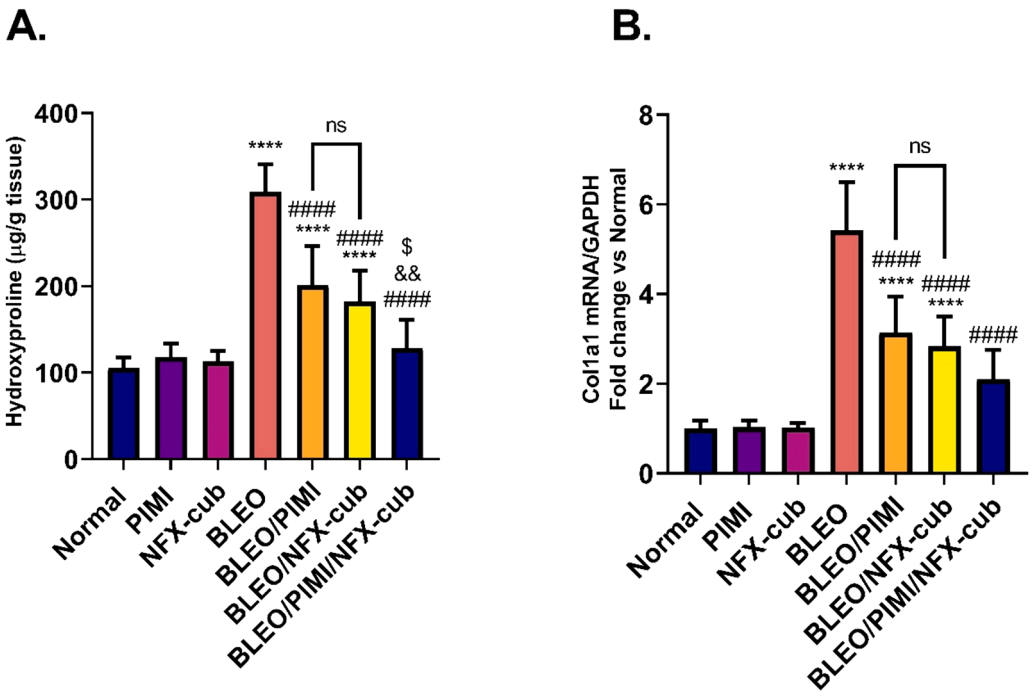

Fig. 3. Effect of pimitespib, nifuroxazide, and their combined therapy on hydroxyproline (A) and the mRNA expression of COL1A1 (B) in lung tissues. $P \leq 0.05$ indicates a statistical significance. * , vs Normal; #, vs BLEO; &, vs BLEO/PIMI; $, vs BLEO/NFX-cub. Levels of significance were used as follows: one symbol, $P \leq 0.05$; two symbols, $P \leq 0.01$; three symbols, $P \leq 0.001$; four symbols, $P \leq 0.0001$.

increased levels of p-mTOR when compared to the normal group. BLEO/NFX-cub and BLEO/PIMI/NFX-cub groups showed a marked reduction in levels of p-mTOR when compared to the BLEO group. However, the BLEO/PIMI group showed a non-significant change in the levels of p-mTOR compared with the BLEO group.

3.10. Effect of pimitespib and/or nifuroxazide on lung sections stained with H&E

As depicted in Fig. 9**A,** Normal and drug control groups (**PIMI and NFX-cub)** display normal lung histology. However, a challenge with bleomycin (**BLEO group**) resulted in severe inflammation and alveolar wall thickening which are reflected as a higher inflammation score (Fig. 9**B**) compared to normal rat lungs. On the other hand, all treatment groups, in particular, the combined therapy group display a marked resolution of the inflammatory signs and a significant reduction in the score.

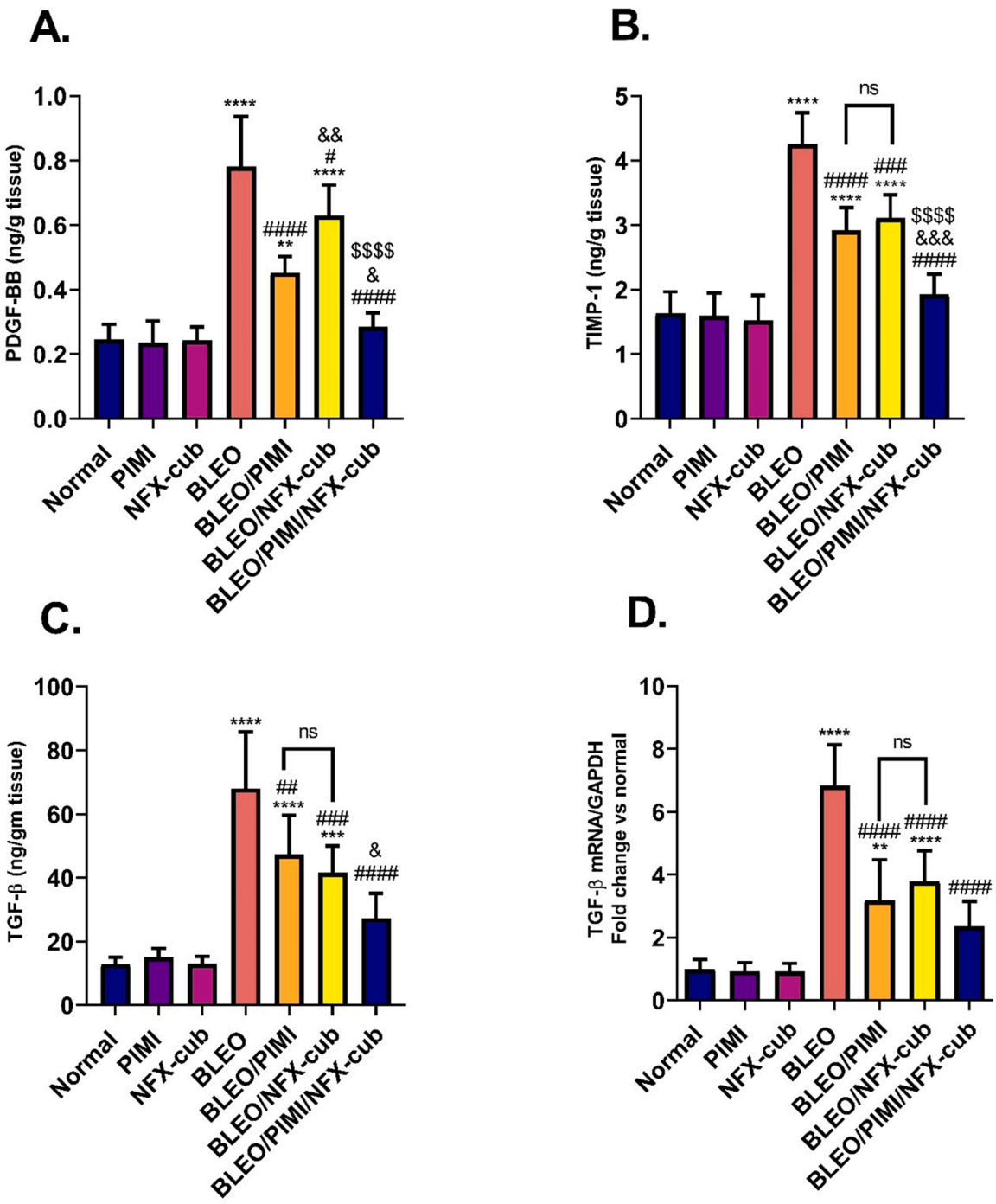

Fig. 4. Effect of pimitespib, nifuroxazide, and their combined therapy on the levels of PDGF-BB (A), TIMP-1 (B), TGF-β (C), and the mRNA expression of TGF-β (D) in lung tissues. $P \leq 0.05$ indicates a statistical significance. * , vs Normal; #, vs BLEO; &, vs BLEO/PIMI; $, vs BLEO/NFX-cub. Levels of significance were used as follows: one symbol, $P \leq 0.05$; two symbols, $P \leq 0.01$; three symbols, $P \leq 0.001$; four symbols, $P \leq 0.0001$.

3.11. Effect of pimitespib and/or nifuroxazide on lung sections stained with Masson trichrome

As depicted in Fig. 9**C and D,** Normal and drug control groups **(PIMI and NFX-cub)** display normal lung structure. However, a challenge with bleomycin (**BLEO group**) resulted in the massive deposition of extracellular matrix components which led to a higher fibrotic score compared to normal rat lungs. On the other hand, all treatment groups, in particular, the combined therapy group display a marked resolution of the fibrotic changes and a significant reduction in the score of fibrosis.

4. Discussion

Pulmonary fibrosis is the last phase of a progressive lung disease affecting the parenchyma and is distinguished by the intensive accumulation of extracellular matrix (ECM) and disruption of the lung structure and function, which in turn results in respiratory failure [34]. IPF is an end-stage disease whose etiology has been a subject of dispute in the preceding few years [35]. In this study, the potential protective effects of pimitespib, nifuroxazide-loaded cubosomes, or their combination against pulmonary fibrosis induced by endotracheal instillation of bleomycin were investigated. Cubosomes, as a drug delivery system,

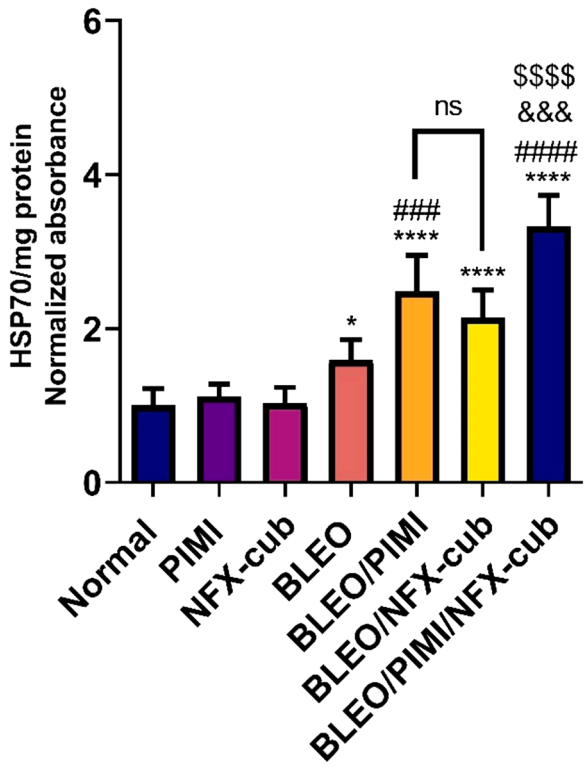

Fig. 5. Effect of pimitespib, nifuroxazide, and their combined therapy on HSP70 levels in lung tissues. $P \leq 0.05$ indicates a statistical significance. * , vs Normal; #, vs BLEO; &, vs BLEO/PIMI; $, vs BLEO/NFX-cub. Levels of significance were used as follows: one symbol, $P \leq 0.05$; two symbols, $P \leq 0.01$; three symbols, $P \leq 0.001$; four symbols, $P \leq 0.0001$.

were proved to increase the oral bioavailability and lung tissue distribution of the poorly soluble drug nifuroxazide [17].

Bleomycin-induced lung fibrosis animal model is commonly used to study IPF [36]. Bleomycin is a chemotherapeutic antibiotic that was identified to induce pulmonary fibrosis in human and multiple animal models [37]. Bleomycin acts by inducing the breakage of DNA double-strands of tumor cells leading to an interruption of the cell cycle and apoptosis [38]. It is inactivated by the bleomycin hydrolase enzyme, which is expressed in low levels in the lungs. Therefore, lungs are believed to be more susceptible to bleomycin-induced injury [39]. In the current model, intra-tracheal instillation of bleomycin produced a marked elevation in total protein levels, total and differential cell counts, NOx (nitrite plus nitrate) content, and LDH activity in the BALF. These findings agree with previous studies which reported increased total protein (reflecting pulmonary edema), total and differential cell counts (representing increased capillary permeability), NOx (related to oxidative stress), and LDH (indicating cytotoxicity) in models of pulmonary fibrosis induced by bleomycin [40,41].

Prolonged inflammation and tissue damage induced by bleomycin consequently promoted proliferation and galvanization of fibroblasts ensued by the accumulation of collagen [42]. Hydroxyproline, the chief constituent of collagen, is measured to reflect collagen synthesis and pulmonary tissue fibrosis [5]. Furthermore, TGF-β is believed to have a crucial role in the progression of fibrosis by aggravating collagen and fibronectin formation from the activated fibroblasts along with inhibiting proteases that decrypt the ECM [43]. TGF-β has been shown to activate the tissue inhibitor of metalloproteinase-1 (TIMP-1), which in turn inhibits matrix metalloproteinase 1 (MMP-1). MMP-1 is able to degrade collagen type I and II, therefore, its inhibition would lead to the subsequent formation of ECM and progression of fibrosis [44]. PDGF-BB is an essential pro-fibrogenic growth factor, which is produced by alveolar macrophages and epithelial cells. It plays a crucial role in the development of myofibroblasts by promoting proliferation, migration, and survival. These myofibroblasts deposit extensive connective tissue products in the alveolar wall resulting in the deterioration of alveolar architecture [45]. Our results showed a bleomycin-induced elevation in hydroxyproline content, gene expression of both Col1A1 and TGF-β, and protein levels of TGF-β, TIMP-1, and PDGF-BB when compared to the normal group. These biochemical findings corroborate the development of interstitial fibrosis in the bleomycin group. The pimitespib- or nifuroxazide-induced reduction in lung collagen as evidenced by reduced gene expression of Col1A1, diminished hydroxyproline content, and minimized collagen fibers distribution in lung sections (Masson's trichrome stain) could be attributed to the inhibitory effects of these drugs on TIMP-1. Their ability to inhibit TIMP-1 could also be attributed to their inhibitory effects on TGF-β1 [46]. Moreover, the significant decrease in protein levels of PDGF-BB by both drugs confirm that they possess anti-fibrotic properties and thereby could combat against bleomycin-induced fibrosis.

The reported decline in pulmonary levels of profibrotic agents after oral treatment with either pimitespib or nifuroxazide or their combination significantly decreased total protein levels, differential cell counts, NOx levels, and LDH activity in the BALF. These results were confirmed by the histopathological findings, which demonstrated that pimitespib and nifuroxazide or their combination attenuated bleomycin-induced inflammation and improved inflammation scoring. These findings also propose that pimitespib or nifuroxazide and particularly their combined therapy might confer protective and anti-inflammatory effects against bleomycin-induced lung injury [17].

HSP90 and HSP70, the ATP-dependent molecular chaperones, are believed to exert several important functions that are essential for the maintenance of protein hemostasis. Their expression is induced in response to cellular stress conditions [47]. Both proteins collaborate with their cochaperones in the remodeling and activation of various proteins [48]. HSP90 expresses multiple binding sites for different client proteins including HIF-1 and STAT3 [49]. Cochaperones also participate in the recruitment of these client proteins leading to the stabilization of HSP90 in an ATP-bound state to prolong the activity of the produced multichaperone complex [50].

Hypoxia participates in the pathogenesis of pulmonary fibrosis and is orchestrated by several transcription factors such as HIF-1α which is released in response to low oxygen levels. HSP90 interacts with HIF-1α and enhances the nuclear translocation and binding of HIF-1α/CREB-p300 HAT to DNA [51,52]. It has been reported that aggravated HIF-1α activity induces cell proliferation and enhances ECM formation, which eventually results in lung inflammation and fibrosis [53]. In our study, there was a significant increase in HIF-1α and CREB-p300 activity in bleomycin-instilled rats. This finding agrees with earlier studies that showed high HIF-1α/CREB activity in pulmonary fibrosis-induced experimentally [5,54,55]. p300 HAT has an essential role in fibrosis and controls the fibrotic response by regulating ECM homeostasis and activation of myofibroblast [56]. It has been reported that p300 mediates TGF-β-induced transcriptional activation of fibrotic genes during pulmonary fibrosis [57]. Also, it has been shown that the expression of active p300 is elevated in IPF patient-derived fibroblasts, which finally resulted in pulmonary fibrosis [58]. STAT3, a protein usually expressed in cells, can be activated by various ligands and plays a pivotal role in the progression of pulmonary fibrosis. STAT3 mediates TGF-β profibrotic pathway to promote fibroblast activation and tissue fibrosis [59]. Moreover, HSP90 showed a crucial role in the regulation of autocrine IL-6 function via direct interaction with STAT3 at its N-terminal region [60,61]. STAT3 interacts with CREB-p300 HAT-binding proteins to form a stable dimer that binds with DNA [62].

Pimitespib is a novel inhibitor of cytosolic HSP90 that leads to significant depletion in several HSP90 proteins [63]. It was developed as an antitumor agent that promotes tumor shrinkage with minimal adverse effects. It was previously reported that HSP70 levels are elevated after administration of HSP90 inhibitors, therefore its upregulation serves as

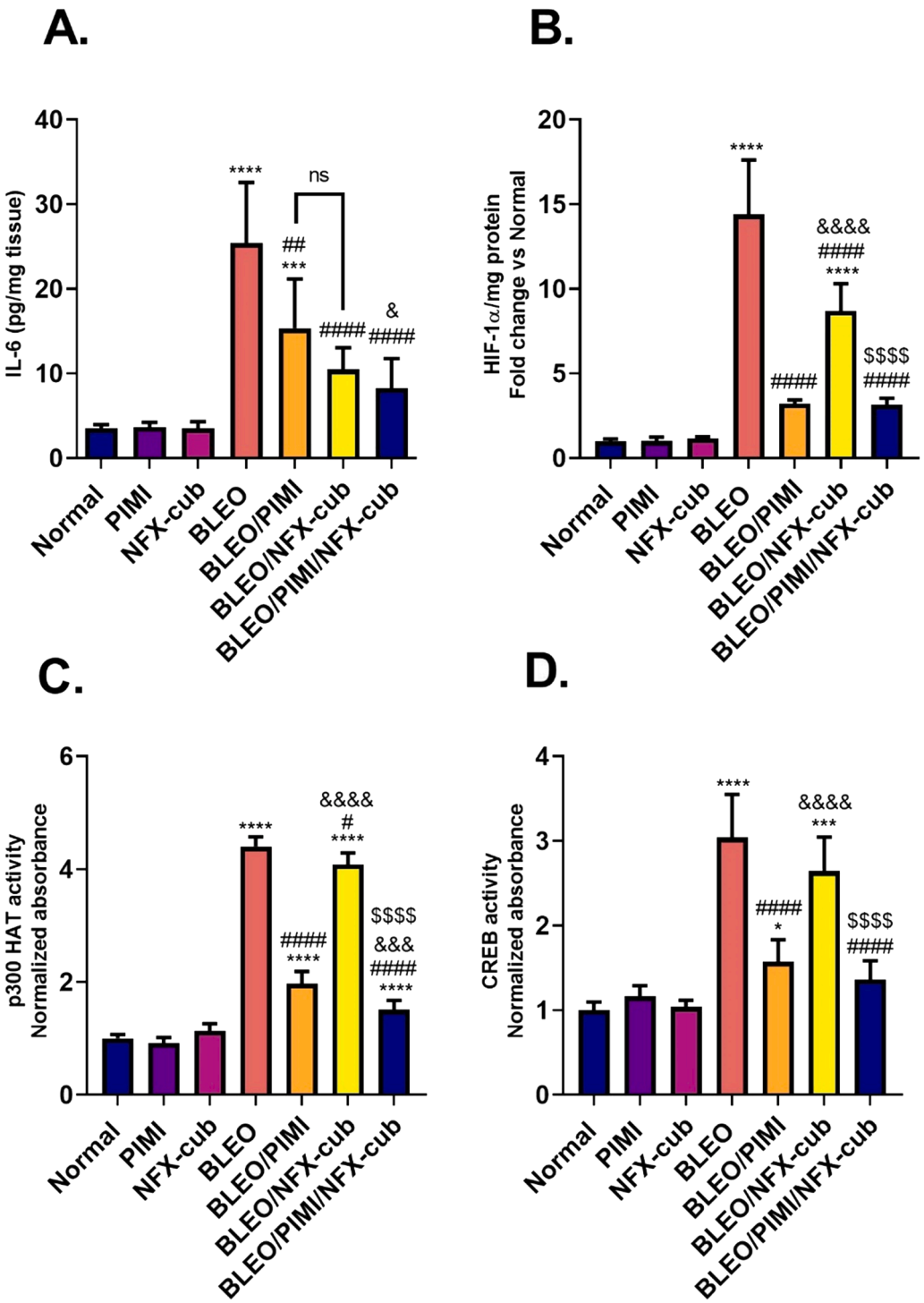

Fig. 6. Effect of pimitespib, nifuroxazide, and their combined therapy on the levels of IL-6 (A), HIF-1α (B), p300 HAT (C), and CREB (D) in lung tissues. $P \leq 0.05$ indicates a statistical significance. * , vs Normal; #, vs BLEO; &, vs BLEO/PIMI; $, vs BLEO/NFX-cub. Levels of significance were used as follows: one symbol, $P \leq 0.05$; two symbols, $P \leq 0.01$; three symbols, $P \leq 0.001$; four symbols, $P \leq 0.0001$.

a surrogate marker for the inhibition of HSP90 function [64,65], which could explain the reported increase in HSP70 levels after treatment with pimitespib in our study. Pimitespib-induced inhibition of HSP90 could lead to subsequent inhibition of HIF-1α and STAT3 client proteins (the closed HSP90 would not enclose its client proteins). Therefore, the inhibition of HSP90 would lead to a subsequent decline in HIF-1α/-CREB-p300 HAT signaling as well as a depression in the pSTAT3/CREB-p300 HAT signaling leading to a reduction in cellular proliferation and ECM formation [66,67]. This could reduce the activation of myofibroblasts leading to further inhibition of pulmonary fibrosis.

Nifuroxazide is an orally administered antibiotic agent that is used for the treatment of diarrhea and colitis [14]. It was previously reported that nifuroxazide could inhibit IL-6/STAT3 axis activation without affecting HSP90 activity [68]. This could explain the notable decline in pSTAT3 levels and the non-significant decrease in HSP90 levels in rats with pulmonary fibrosis and treated with nifuroxazide. Additionally, after treatment with nifuroxazide, our results showed a significant

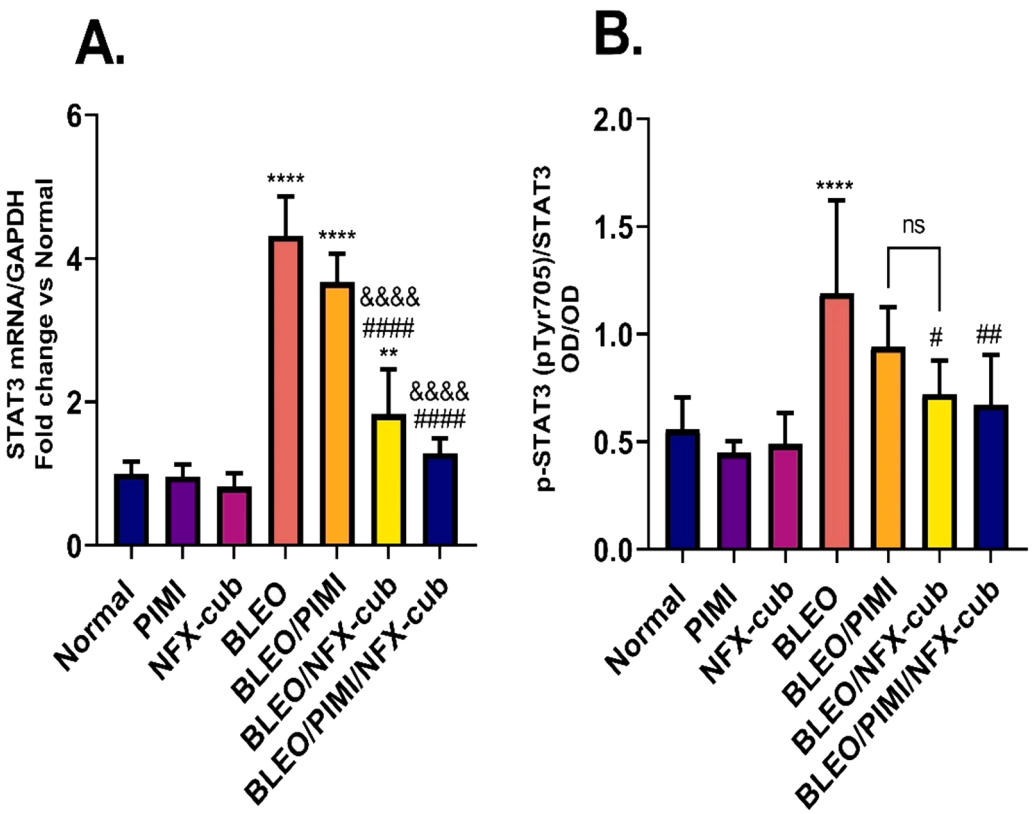

Fig. 7. Effect of pimitespib, nifuroxazide, and their combined therapy on the mRNA expression of STAT3 (A) and the levels of normalized p-STAT3 (B) in lung tissues. $P \leq 0.05$ indicates a statistical significance. * , vs Normal; #, vs BLEO; &, vs BLEO/PIMI. Levels of significance were used as follows: one symbol, $P \leq 0.05$; two symbols, $P \leq 0.01$; three symbols, $P \leq 0.001$; four symbols, $P \leq 0.0001$.

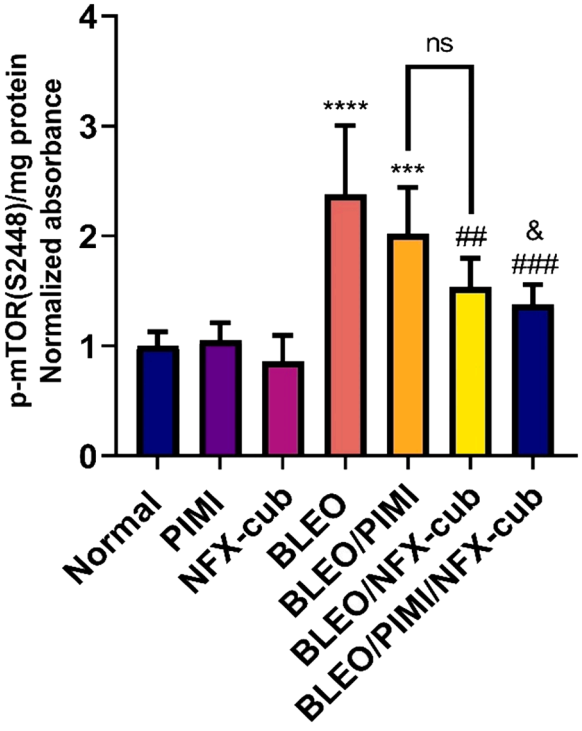

Fig. 8. Effect of pimitespib, nifuroxazide, and their combined therapy on p-mTOR in lung tissues. $P \leq 0.05$ indicates a statistical significance. * , vs Normal; #, vs BLEO; &, vs BLEO/PIMI. Levels of significance were used as follows: one symbol, $P \leq 0.05$; two symbols, $P \leq 0.01$; three symbols, $P \leq 0.001$; four symbols, $P \leq 0.0001$.

decrease in HIF-1α levels compared to the levels of bleomycin-instilled rats. One report findings suggest that STAT3 is a potential target for intervention in pathologies where there is hypoxia and that STAT3 precedes HIF-1α transcriptional responses to oxygen [69]. Additionally, Activated STAT3 has been described as a positive regulator of HIF-1α [70,71]. Indeed, phospho STAT3 increases the expression of HIF-1α by inhibiting its degradation in tumor cells [72]. Another report suggested that STAT3 is a superior target for the development of anticancer drugs when authors found that STAT3 enhances HIF-1α protein stability through inhibition of pVHL binding to the HIF-1α and pVHL-mediated ubiquitination of HIF-1α [73]. Also, it was hypothesized that STAT3 is a general co-transcription factor of the HIF-mediated hypoxia response [74]. These perspectives are supported by our findings where HIF-1α levels were downregulated in response to nifuroxazide treatment.

Compelling evidence by Lang, et al. [75] supports the presence of the IL-6/STAT3/HIF-1α autocrine loop in which authors showed that HSP90 inhibitors can disrupt the HIF-1α/STAT3 mediated autocrine activation loop for IL-6 by direct hindrance with the functions of HIF-1α and STAT3. In this regard, pimitespib disrupted the IL-6/STAT3/HIF-1α autocrine loop in rats with pulmonary fibrosis in our study. This resulted in inhibition of the nuclear translocation of either STAT3 or HIF-1α. Pimitespib, as an adjuvant to nifuroxazide, downregulated both HIF-1α and pSTAT3 to augment the nifuroxazide inhibitory function.

It is believed that mTOR is aberrantly triggered in fibrotic diseases, such as lung fibrosis [76]. In the present study, nifuroxazide showed a potential to induce autophagy in fibrotic lungs as indicated by decreased levels of p-mTOR. However, this effect needs further investigation. On the other hand, pimitespib-induced inhibition of HSP90 did not result in a significant decrease in the pmTOR levels [77,78]. This could be due to the reported non-significant effect of pimitespib on the pSTAT3 levels in rats with pulmonary fibrosis compared to the bleomycin group. It is well acknowledged that the pmTOR levels are correlated with pSTAT3 levels

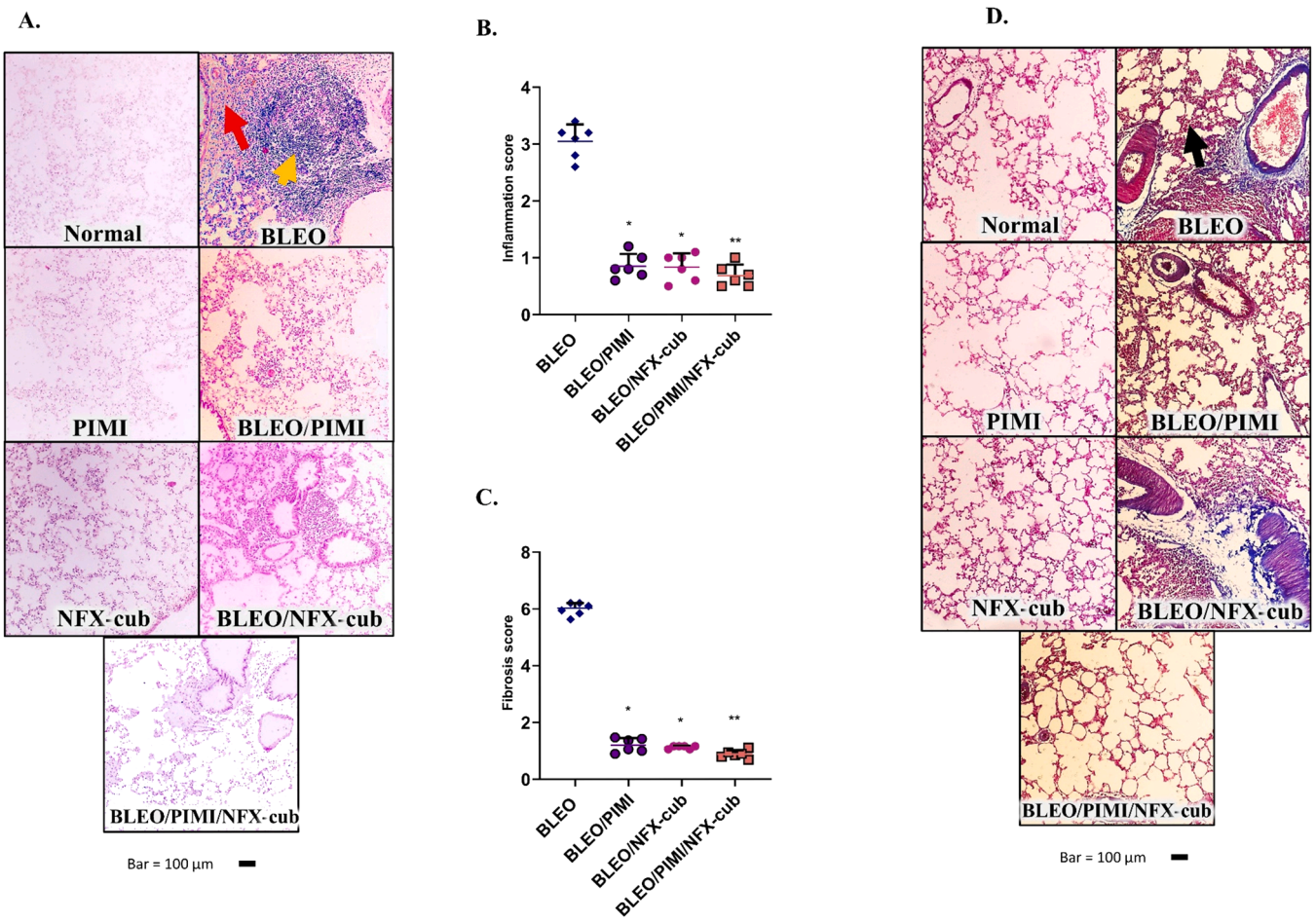

Fig. 9. Effect of pimitespib and/or nifuroxazide on lung sections stained with H&E stain (A); inflammation score (B); fibrosis score (C) and lung sections stained with Masson trichrome stain (D). The short orange arrow indicates massive inflammatory cell infiltration and the long red arrow indicates fibrotic tissue deposition (Figure A; BLEO group). On the other hand, the long black arrow indicates fibrotic mass deposition (Figure D; BLEO group). $P \leq 0.05$ indicates a statistical significance. * , vs Normal; #, vs BLEO; &, vs BLEO/PIMI; $, vs BLEO/NFX-cub. Levels of significance were used as follows: one symbol, $P \leq 0.05$; two symbols, $P \leq 0.01$; three symbols, $P \leq 0.001$; four symbols, $P \leq 0.0001$.

and that mTOR can activate the pSTAT3 signaling cascade [79]. Therefore, pimitespib could reduce the HSP90 ATP binding and nuclear translocation of pSTAT3 without reducing pSTAT3 or pmTOR levels.

In conclusion, the current study proposed that pimitespib/nifuroxazide inhibited bleomycin-induced alterations in either the structure or the function of the lungs and this impact was mediated via inhibiting the nuclear translocation of HIF-1α and pSTAT3. This is followed by the inhibition of STAT3/CREB-p300 HAT and HIF-1α/CREB-P300 HAT nuclear interactions. Herein, Pimitespib augmented nifuroxazide-induced disruption in the IL-6/STAT3/HIF-1α autocrine loop in rats. Our findings disclose that the IL-6/STAT3/HIF-1α autocrine loop is a promising therapeutic attack site for possible pulmonary fibrosis repression studies. Therefore, the use of pimitespib/nifuroxazide embodies an evolutionary perspective in managing pulmonary fibrosis. However, extensive applications in view of other potential downstream effects of HSP90 inhibition in the context of STAT3 inhibition, are still to be characterized. In addition, demonstration of the efficacy and safety of the combined therapy of HSP90 and STAT3 inhibitors awaits further evaluation.

CRediT authorship contribution statement

Conceptualization, methodology, software, validation, formal analysis, investigation, resources, writing - review & editing and project administration were performed by Sameh Saber. Methodology, software, statistical analysis, writing - original draft, and writing - review & editing were performed by Dalia H. El-Kashef, Mahmoud E. Youssef, Mohamed Nasr, Mohammed Alrouji, Sharif Alhajlah, and Othman AlOmeir. Methodology, software, validation, formal analysis, resources, and writing - review & editing were performed by Noura El Adle Khalaf, Osama A. Mohammed, Dalia M. Abdel Ghaffar, Lubna Jamil, Zeinab M. Abdel-Nasser, Samar Ibrahim, Mahmoud Said Ibrahim Abdeldaiem, Sally S. Donia, Ahmed Shata, Nesreen Elsayed Morsy.

Declaration of Competing Interest

The authors declare that they have no known competing financial interests or personal relationships that could have appeared to influence the work reported in this paper.

Data availability

Data will be made available on request.

Acknowledgment

The authors would like to thank the Deanship of Scientific Research at Shaqra University for supporting this work.

References

[1] T.J. Gross, G.W. Hunninghake, Idiopathic pulmonary fibrosis, New Engl. J. Med. 345 (7) (2001) 517–525.

[2] E.E. Abd El-Fattah, S. Saber, A.A.E. Mourad, E. El-Ahwany, N.A. Amin, S. Cavalu, G. Yahya, A.S. Saad, M. Alsharidah, A. Shata, H.M. Sami, M.M.Y. Kaddah, A.M. H. Ghanim, The dynamic interplay between AMPK/NFκB signaling and NLRP3 is a new therapeutic target in inflammation: Emerging role of dapagliflozin in overcoming lipopolysaccharide-mediated lung injury, Biomed. Pharmacother. 147 (2022), 112628.

[3] M.K. Tawfik, S. Makary, 5-HT7 receptor antagonism (SB-269970) attenuates bleomycin-induced pulmonary fibrosis in rats via downregulating oxidative burden and inflammatory cascades and ameliorating collagen deposition: Comparison to terguride, Eur. J. Pharmacol. 814 (2017) 114–123.

[4] M. Selman, T.E. King, A. Pardo, Idiopathic pulmonary fibrosis: prevailing and evolving hypotheses about its pathogenesis and implications for therapy, Ann. Intern. Med. 134 (2) (2001) 136–151.

[5] M.O. Kseibati, G.S.G. Shehatou, M.H. Sharawy, A.E. Eladl, H.A. Salem, Nicorandil ameliorates bleomycin-induced pulmonary fibrosis in rats through modulating eNOS, iNOS, TXNIP and HIF-1α levels, Life Sci. 246 (2020), 117423.

[6] P.M. George, A.U. Wells, R.G. Jenkins, Pulmonary fibrosis and COVID-19: the potential role for antifibrotic therapy, Lancet Respir. Med. 8 (8) (2020) 807–815.

[7] S. Kayhan, A. Guzel, L. Duran, S. Tutuncu, A. Guzel, M. Gunaydın, O. Salis, A. Okuyucu, M.Y. Selcuk, Effects of leflunomide on inflamation and fibrosis in bleomycine induced pulmonary fibrosis in wistar albino rats, J. Thorac. Dis. 5 (5) (2013) 641–649.

[8] T. Liu, F.G. De Los Santos, S.H. Phan, The bleomycin model of pulmonary fibrosis, Methods Mol. Biol. (Clifton, N. J.) 1627 (2017) 27–42.

[9] H. Zhao, C. Li, L. Li, J. Liu, Y. Gao, K. Mu, D. Chen, A. Lu, Y. Ren, Z. Li, Baicalin alleviates bleomycin-induced pulmonary fibrosis and fibroblast proliferation in rats via the PI3K/AKT signaling pathway, Mol. Med. Rep. 21 (6) (2020) 2321–2334.

[10] S. Saber, E.E. Abd El-Fattah, G. Yahya, N.A. Gobba, A.O. Maghmomeh, A.E. Khodir, A.A.E. Mourad, A.S. Saad, H.G. Mohammed, N.A. Nouh, A. Shata, N.A. Amin, M. Abou El-Rous, S. Girgis, E. El-Ahwany, E.M. Khalaf, A.F. El-Kott, A.M. El-Baz, A novel combination therapy using rosuvastatin and lactobacillus combats dextran sodium sulfate-induced colitis in high-fat diet-fed rats by targeting the TXNIP/NLRP3 interaction and influencing gut microbiome composition, Pharmaceuticals 14 (4) (2021).

[11] S. Saber, G. Yahya, N.A. Gobba, H. Sharaf, R. Alshaman, A. Alattar, N.A. Amin, R. El-Shedody, F.H. Aboutouk, Y. Abd El-Galeel, A. El-Hefnawy, D. Shabaka, A. Khalifa, R. Saleh, D. Osama, G. El-Zoghby, M.E. Youssef, The supportive role of NSC328382, a P2X7R antagonist, in enhancing the inhibitory effect of crid3 on nlrp3 inflammasome activation in rats with dextran sodium sulfate-induced colitis, J. Inflamm. Res 14 (2021) 3443–3463.

[12] F. Saito, S. Tasaka, K. Inoue, K. Miyamoto, Y. Nakano, Y. Ogawa, W. Yamada, Y. Shiraishi, N. Hasegawa, S. Fujishima, H. Takano, A. Ishizaka, Role of interleukin-6 in bleomycin-induced lung inflammatory changes in mice, Am. J. Respir. Cell Mol. Biol. 38 (5) (2008) 566–571.

[13] Y. Zhou, J.N. Murthy, D. Zeng, L. Belardinelli, M.R. Blackburn, Alterations in adenosine metabolism and signaling in patients with chronic obstructive pulmonary disease and idiopathic pulmonary fibrosis, PloS One 5 (2) (2010), e9224.

[14] C. Bailly, Toward a repositioning of the antibacterial drug nifuroxazide for cancer treatment, Drug Discov. Today 24 (9) (2019) 1930–1936.

[15] E.A. Nelson, S.R. Walker, A. Kepich, L.B. Gashin, T. Hideshima, H. Ikeda, D. Chauhan, K.C. Anderson, D.A. Frank, Nifuroxazide inhibits survival of multiple myeloma cells by directly inhibiting STAT3, Blood 112 (13) (2008) 5095–5102.

[16] C. Gan, Q. Zhang, H. Liu, G. Wang, L. Wang, Y. Li, Z. Tan, W. Yin, Y. Yao, Y. Xie, L. Ouyang, L. Yu, T. Ye, Nifuroxazide ameliorates pulmonary fibrosis by blocking myofibroblast genesis: a drug repurposing study, 23(1) (2022) 32.

[17] S. Saber, M. Nasr, M.M.Y. Kaddah, G. Mostafa-Hedeab, S. Cavalu, A.A.E. Mourad, A.G.A. Gaafar, S.S. Zaghlool, S. Saleh, M.M. Hafez, S. Girgis, R.M. Elgharabawy, K. Nader, M. Alsharidah, G.E.-S. Batiha, E. El-Ahwany, N.A. Amin, H.I. Elagamy, A. Shata, R. Nader, A.E. Khodir, Nifuroxazide-loaded cubosomes exhibit an advancement in pulmonary delivery and attenuate bleomycin-induced lung fibrosis by regulating the STAT3 and NF-κB signaling: a new challenge for unmet therapeutic needs, Biomed. Pharmacother. 148 (2022), 112731.

[18] J. Goodwin, H. Choi, M.H. Hsieh, M.L. Neugent, J.M. Ahn, H.N. Hayenga, P. K. Singh, D.B. Shackelford, I.K. Lee, V. Shulaev, S. Dhar, N. Takeda, J.W. Kim, Targeting hypoxia-inducible factor-1α/pyruvate dehydrogenase kinase 1 axis by dichloroacetate suppresses bleomycin-induced pulmonary fibrosis, Am. J. Respir. Cell Mol. Biol. 58 (2) (2018) 216–231.

[19] S. Saber, M. Nasr, A.S. Saad, A.A.E. Mourad, N.A. Gobba, A. Shata, A.-M. Hafez, R. N. Elsergany, H.I. Elagamy, E. El-Ahwany, N.A. Amin, S. Girgis, Y.H.A. Elewa, M. H. Mahmoud, G.E.-S. Batiha, M.A. El-Rous, I. Kamal, M.M.Y. Kaddah, A.E. Khodir, Albendazole-loaded cubosomes interrupt the ERK1/2-HIF-1α-p300/CREB axis in mice intoxicated with diethylnitrosamine: A new paradigm in drug repurposing for the inhibition of hepatocellular carcinoma progression, Biomed. Pharmacother. 142 (2021), 112029.

[20] T. Uno, Y. Kawai, S. Yamashita, H. Oshiumi, C. Yoshimura, T. Mizutani, T. Suzuki, K.T. Chong, K. Shigeno, M. Ohkubo, Y. Kodama, H. Muraoka, K. Funabashi, K. Takahashi, S. Ohkubo, M. Kitade, Discovery of 3-Ethyl-4-(3-isopropyl-4-(4-(1-methyl-1H-pyrazol-4-yl)-1H-imidazol-1-yl)-1H-pyrazolo[3,4-b]pyridin-1-yl)benzamide (TAS-116) as a potent, selective, and orally available HSP90 inhibitor, J. Med. Chem. 62 (2) (2019) 531–551.

[21] S. Ohkubo, Y. Kodama, H. Muraoka, H. Hitotsumachi, C. Yoshimura, M. Kitade, A. Hashimoto, K. Ito, A. Gomori, K. Takahashi, Y. Shibata, A. Kanoh, K. Yonekura, TAS-116, a highly selective inhibitor of heat shock protein 90α and β, demonstrates potent antitumor activity and minimal ocular toxicity in preclinical models, Mol. Cancer Ther. 14 (1) (2015) 14–22.

[22] E. Ikebe, S. Shimosaki, H. Hasegawa, TAS-116 (pimitespib), a heat shock protein 90 inhibitor, shows efficacy in preclinical models of adult T-cell leukemia, (2021).

[23] P. Solopov, R. Biancatelli, M. Marinova, C. Dimitropoulou, J.D. Catravas, The HSP90 inhibitor, AUY-922, ameliorates the development of nitrogen mustard-induced pulmonary fibrosis and lung dysfunction in mice, Int. J. Mol. Sci. 21 (13) (2020).

[24] R.M.L. Colunga Biancatelli, P. Solopov, C. Dimitropoulou, B. Gregory, T. Day, J. D. Catravas, The heat shock protein 90 inhibitor, AT13387, protects the alveolo-capillary barrier and prevents HCl-induced chronic lung injury and pulmonary fibrosis, Cells 11 (6) (2022).

[25] A. Ntranos, P. Casaccia, Bromodomains: translating the words of lysine acetylation into myelin injury and repair, Neurosci. Lett. 625 (2016) 4–10.

[26] Y. Zhang, U. Bharadwaj, C.D. Logsdon, C. Chen, Q. Yao, M. Li, ZIP4 regulates pancreatic cancer cell growth by activating IL-6/STAT3 pathway through zinc finger transcription factor CREB, Clin. Cancer Res. 16 (5) (2010) 1423–1430.

[27] F. Wang, R. Zhang, X. Wu, O. Hankinson, Roles of coactivators in hypoxic induction of the erythropoietin gene, PLOS ONE 5 (4) (2010), e10002.

[28] P. Carrero, K. Okamoto, P. Coumailleau, S. O'Brien, H. Tanaka, L. Poellinger, Redox-regulated recruitment of the transcriptional coactivators CREB-binding protein and SRC-1 to hypoxia-inducible factor 1α, Mol. Cell. Biol. 20 (1) (2000) 402–415.

[29] M.E. Youssef, M.F. El-Azab, M.A. Abdel-Dayem, G. Yahya, I.S. Alanazi, S. Saber, Electrocardiographic and histopathological characterizations of diabetic cardiomyopathy in rats, Environ. Sci. Pollut. Res. Int. 29 (17) (2022) 25723–25732.

[30] M. Nasr, M. Teiama, A. Ismail, A. Ebada, S. Saber, In vitro and in vivo evaluation of cubosomal nanoparticles as an ocular delivery system for fluconazole in treatment of keratomycosis, Drug Deliv. Transl. Res. (2020).

[31] R.-H. Hübner, W. Gitter, N. Eddine El Mokhtari, M. Mathiak, M. Both, H. Bolte, S. Freitag-Wolf, B. Bewig, Standardized quantification of pulmonary fibrosis in histological samples, BioTechniques 44 (4) (2008) 507–517.

[32] M.A. El-Rous, S. Saber, E.M. Raafat, A.A.E. Ahmed, Dapagliflozin, an SGLT2 inhibitor, ameliorates acetic acid-induced colitis in rats by targeting NFκB/AMPK/NLRP3 axis, Inflammopharmacology (2021).

[33] M.E. Youssef, E.E. Abd El-Fattah, A.M. Abdelhamid, H. Eissa, E. El-Ahwany, N.A. Amin, H.F. Hetta, M.H. Mahmoud, G.E.-S. Batiha, N. Gobba, A.G. Ahmed Gaafar, S. Saber, Interference With the AMPKα/mTOR/NLRP3 Signaling and the IL-23/IL-17 Axis Effectively Protects Against the Dextran Sulfate Sodium Intoxication in Rats: A New Paradigm in Empagliflozin and Metformin Reprofiling for the Management of Ulcerative Colitis, 12 (2021).

[34] P.W. Noble, C.E. Barkauskas, D. Jiang, Pulmonary fibrosis: patterns and perpetrators, The, J. Clin. Investig. 122 (8) (2012) 2756–2762.

[35] T.E. King Jr., A. Pardo, M. Selman, Idiopathic pulmonary fibrosis, Lancet (Lond., Engl.) 378 (9807) (2011), 1949-61.

[36] A. Moeller, K. Ask, D. Warburton, J. Gauldie, M. Kolb, The bleomycin animal model: a useful tool to investigate treatment options for idiopathic pulmonary fibrosis? Int. J. Biochem. Cell Biol. 40 (3) (2008) 362–382.

[37] T. Liu, F.G.D. Los Santos, S.H. Phan, The bleomycin model of pulmonary fibrosis, Fibrosis, Springer (2017) 27–42.

[38] Y. Gao, Q. Shang, W. Li, W. Guo, A. Stojadinovic, C. Mannion, T.Chen Y.-g. Man, Antibiotics for cancer treatment: A double-edged sword, Journal of Cancer 11 (17) (2020) 5135.

[39] J.S. Lazo, C.J. Humphreys, Lack of metabolism as the biochemical basis of bleomycin-induced pulmonary toxicity, Proc. Natl. Acad. Sci. 80 (10) (1983) 3064–3068.

[40] M.S. Zaghloul, E. Said, G.M. Suddek, H.A. Salem, Crocin attenuates lung inflammation and pulmonary vascular dysfunction in a rat model of bleomycin-induced pulmonary fibrosis, Life Sci. 235 (2019), 116794.

[41] P. Almudéver, J. Milara, A. De Diego, A. Serrano-Mollar, A. Xaubet, F. Perez-Vizcaino, A. Cogolludo, J. Cortijo, Role of tetrahydrobiopterin in pulmonary vascular remodelling associated with pulmonary fibrosis, Thorax 68 (10) (2013) 938.

[42] V. Della Latta, A. Cecchettini, S. Del, Ry Morales M.A., Bleomycin in the setting of lung fibrosis induction: From biological mechanisms to counteractions, Pharmacol. Res. 97 (2015) 122–130.

[43] L.A. Ahmed, S.A. El-Maraghy, S.M. Rizk, Role of the KATP channel in the protective effect of nicorandil on cyclophosphamide-induced lung and testicular toxicity in rats, Sci. Rep. 5 (2015) 14043.

[44] A. Pardo, M. Selman, Role of matrix metaloproteases in idiopathic pulmonary fibrosis, Fibrogenes. Tissue Repair 5 (Suppl 1) (2012) S9.

[45] L. Wollin, I. Maillet, V. Quesniaux, A. Holweg, B. Ryffel, Antifibrotic and anti-inflammatory activity of the tyrosine kinase inhibitor nintedanib in experimental models of lung fibrosis, J. Pharmacol. Exp. Ther. 349 (2) (2014) 209–220.

[46] M. Profita, R. Gagliardo, R. Di Giorgi, A. Bruno, L. Riccobono, A. Bonanno, J. Bousquet, A. Vignola, In vitro effects of flunisolide on MMP-9, TIMP-1, fibronectin, TGF-β1 release and apoptosis in sputum cells freshly isolated from mild to moderate asthmatics, Allergy 59 (9) (2004) 927–932.

[47] R.M.L. Colunga Biancatelli, P. Solopov, B. Gregory, J.D. Catravas, HSP90 inhibition and modulation of the proteome: therapeutical implications for idiopathic pulmonary fibrosis (IPF), Int. J. Mol. Sci. 21 (15) (2020) 5286.

[48] O. Genest, J.R. Hoskins, A.N. Kravats, S.M. Doyle, S. Wickner, Hsp70 and Hsp90 of E. coli directly interact for collaboration in protein remodeling, J. Mol. Biol. 427 (24) (2015) 3877–3889.
[49] H.L. Kim, M. Cassone, L. Otvos Jr., P. Vogiatzi, HIF-1α and STAT3 client proteins interacting with the cancer chaperone Hsp90: Therapeutic considerations, Cancer Biol. Ther. 7 (1) (2008) 10–14.
[50] L. Whitesell, S.L. Lindquist, HSP90 and the chaperoning of cancer, Nat. Rev. Cancer 5 (10) (2005) 761–772.
[51] Q. Tong, M.R. Weaver, E.A. Kosmacek, B.P. O'Connor, L. Harmacek, S. Venkataraman, R.E. Oberley-Deegan, MnTE-2-PyP reduces prostate cancer growth and metastasis by suppressing p300 activity and p300/HIF-1/CREB binding to the promoter region of the PAI-1 gene, Free Radic. Biol. Med. 94 (2016) 185–194.
[52] E. Minet, D. Mottet, G. Michel, I. Roland, M. Raes, J. Remacle, C. Michiels, Hypoxia-induced activation of HIF-1: role of HIF-1α-Hsp90 interaction, FEBS Lett. 460 (2) (1999) 251–256.
[53] H. Huang, X. Wang, X. Zhang, H. Wang, W. Jiang, Roxadustat attenuates experimental pulmonary fibrosis in vitro and in vivo, Toxicol. Lett. 331 (2020) 112–121.
[54] A. Tzouvelekis, V. Harokopos, T. Paparountas, N. Oikonomou, A. Chatziioannou, G. Vilaras, E. Tsiambas, A. Karameris, D. Bouros, V. Aidinis, Comparative expression profiling in pulmonary fibrosis suggests a role of hypoxia-inducible factor-1alpha in disease pathogenesis, Am. J. Respir. Crit. Care Med. 176 (11) (2007) 1108–1119.
[55] C.A. Barlow, T.F. Barrett, A. Shukla, B.T. Mossman, K.M. Lounsbury, Asbestos-mediated CREB phosphorylation is regulated by protein kinase A and extracellular signal-regulated kinases 1/2, Am. J. Physiol. Lung Cell. Mol. Physiol. 292 (6) (2007) L1361–L1369.
[56] T.E. Duong, J.S. Hagood, Epigenetic regulation of myofibroblast phenotypes in fibrosis, Curr. Pathobiol. Rep. 6 (1) (2018) 79–96.
[57] S. Lee, M. Kim, S. Jang, G.-E. Lee, S.-Y. Hwang, Y. Kwon, J. Hong, M. Sohn, S.-Y. Park, H.-G. Yoon, Plumbagin suppresses pulmonary fibrosis via inhibition of p300 histone acetyltransferase activity, J. Med. Food 23 (2020).
[58] K. Rubio, I. Singh, S. Dobersch, Inactivation of nuclear histone deacetylases by EP300 disrupts the MiCEE complex in idiopathic pulmonary fibrosis 10 (1) (2019) 2229.
[59] D. Chakraborty, B. Šumová, T. Mallano, C.W. Chen, A. Distler, C. Bergmann, I. Ludolph, R.E. Horch, K. Gelse, A. Ramming, O. Distler, G. Schett, L. Šenolt, J.H. W. Distler, Activation of STAT3 integrates common profibrotic pathways to promote fibroblast activation and tissue fibrosis, Nat. Commun. 8 (1) (2017) 1130.
[60] N. Sato, T. Yamamoto, Y. Sekine, T. Yumioka, A. Junicho, H. Fuse, T. Matsuda, Involvement of heat-shock protein 90 in the interleukin-6-mediated signaling pathway through STAT3, Biochem. Biophys. Res. Commun. 300 (4) (2003) 847–852.
[61] L. Sreenivasan, H. Wang, S.Q. Yap, P. Leclair, A. Tam, C.J. Lim, Autocrine IL-6/STAT3 signaling aids development of acquired drug resistance in Group 3 medulloblastoma, Cell Death Dis. 11 (12) (2020) 1–15.
[62] H. Wang, M.P. Holloway, L. Ma, Z.A. Cooper, M. Riolo, A. Samkari, K.S. Elenitoba-Johnson, Y.E. Chin, R.A. Altura, Acetylation directs survivin nuclear localization to repress STAT3 oncogenic activity, J. Biol. Chem. 285 (46) (2010) 36129–36137.
[63] E. Ikebe, S. Shimosaki, H. Hasegawa, H. Iha, Y. Tsukamoto, Y. Wang, D. Sasaki, Y. Imaizumi, Y. Miyazaki, K. Yanagihara, TAS-116 (pimitespib), a heat shock protein 90 inhibitor, shows efficacy in preclinical models of adult T-cell leukemia, Cancer Sci. 113 (2) (2022) 684.
[64] H. Taniguchi, H. Hasegawa, D. Sasaki, K. Ando, Y. Sawayama, Y. Imaizumi, D. Imanishi, J. Taguchi, T. Hata, K. Tsukasaki, K. Yanagihara, N. Mori, Y. Miyazaki, Heat shock protein 90 inhibitor NVP-AUY922 has potent anti-tumor activity with adult T-cell leukemia-lymphoma cells, Blood 122 (21) (2013), 1829-1829.
[65] J.C. Friedland, D.L. Smith, J. Sang, J. Acquaviva, S. He, C. Zhang, D.A. Proia, Targeted inhibition of Hsp90 by ganetespib is effective across a broad spectrum of breast cancer subtypes, Investig. N. Drugs 32 (1) (2014) 14–24.
[66] A. Seiferth, S. Ruhs, S. Mildenberger, M. Gekle, C. Grossmann, The phosphatase calcineurin PP2BAβ mediates part of mineralocorticoid receptor transcriptional activity, FASEB J. 26 (6) (2012) 2327–2337.
[67] S.H. Lee, J.G. Jee, J.S. Bae, K.H. Liu, Y.M. Lee, A group of novel HIF-1α inhibitors, glyceollins, blocks HIF-1α synthesis and decreases its stability via inhibition of the PI3K/AKT/mTOR pathway and Hsp90 binding, J. Cell. Physiol. 230 (4) (2015) 853–862.
[68] F.E. Ali, M.M. Elfiky, W.A. Fadda, H.S. Ali, A.R. Mahmoud, Z.M. Mohammedsaleh, T.H. Abd-Elhamid, Regulation of IL-6/STAT-3/Wnt axis by nifuroxazide dampens colon ulcer in acetic acid-induced ulcerative colitis model: Novel mechanistic insight, Life Sci. 276 (2021), 119433.
[69] R. Carlsson, I. Özen, M. Barbariga, A. Gaceb, M. Roth, G. Paul, STAT3 precedes HIF1α transcriptional responses to oxygen and oxygen and glucose deprivation in human brain pericytes, PLoS One 13 (3) (2018), e0194146.
[70] M.J. Gray, J. Zhang, L.M. Ellis, G.L. Semenza, D.B. Evans, S.S. Watowich, G. E. Gallick, HIF-1alpha, STAT3, CBP/p300 and Ref-1/APE are components of a transcriptional complex that regulates Src-dependent hypoxia-induced expression of VEGF in pancreatic and prostate carcinomas, Oncogene 24 (19) (2005) 3110–3120.
[71] J.E. Jung, H.G. Lee, I.H. Cho, D.H. Chung, S.H. Yoon, Y.M. Yang, J.W. Lee, S. Choi, J.W. Park, S.K. Ye, M.H. Chung, STAT3 is a potential modulator of HIF-1-mediated VEGF expression in human renal carcinoma cells, Faseb J. 19 (10) (2005) 1296–1298.
[72] J.E. Jung, H.S. Kim, C.S. Lee, Y.J. Shin, Y.N. Kim, G.H. Kang, T.Y. Kim, Y.S. Juhnn, S.J. Kim, J.W. Park, S.K. Ye, M.H. Chung, STAT3 inhibits the degradation of HIF-1alpha by pVHL-mediated ubiquitination, Exp. Mol. Med. 40 (5) (2008) 479–485.
[73] J.E. Jung, H.S. Kim, C.S. Lee, Y.-J. Shin, Y.-N. Kim, G.-H. Kang, T.-Y. Kim, Y.-S. Juhnn, S.-J. Kim, J.-W. Park, S.-K. Ye, M.-H. Chung, STAT3 inhibits the degradation of HIF-1α by pVHL-mediated ubiquitination, Exp. Mol. Med. 40 (5) (2008) 479–485.
[74] M.R. Pawlus, L. Wang, C.J. Hu, STAT3 and HIF1α cooperatively activate HIF1 target genes in MDA-MB-231 and RCC4 cells, Oncogene 33 (13) (2014) 1670–1679.
[75] S.A. Lang, C. Moser, A. Gaumann, D. Klein, G. Glockzin, F.C. Popp, M.H. Dahlke, P. Piso, H.J. Schlitt, E.K. Geissler, O. Stoeltzing, Targeting heat shock protein 90 in pancreatic cancer impairs insulin-like growth factor-I receptor signaling, disrupts an interleukin-6/signal-transducer and activator of transcription 3/hypoxia-inducible factor-1alpha autocrine loop, and reduces orthotopic tumor growth, Clinical cancer research: an official journal of the American Association for, Cancer Res. 13 (21) (2007) 6459–6468.
[76] Q. Han, L. Lin, B. Zhao, N. Wang, X. Liu, Inhibition of mTOR ameliorates bleomycin-induced pulmonary fibrosis by regulating epithelial-mesenchymal transition, Biochem. Biophys. Res. Commun. 500 (4) (2018) 839–845.
[77] J.J. Barrott, T.A. Haystead, Hsp90, an unlikely ally in the war on cancer, The, FEBS J. 280 (6) (2013) 1381–1396.
[78] B. Ou, H. Sun, J. Zhao, Z. Xu, Y. Liu, H. Feng, Z. Peng, Polo-like kinase 3 inhibits glucose metabolism in colorectal cancer by targeting HSP90/STAT3/HK2 signaling, J. Exp. Clin. Cancer Res. 38 (1) (2019) 1–12.
[79] M. Inokuchi, T. Murayama, M. Hayashi, Y. Takagi, K. Kato, M. Enjoji, K. Kojima, J. Kumagai, K. Sugihara, Prognostic value of co-expression of STAT3, mTOR and EGFR in gastric cancer, Exp. Ther. Med. 2 (2) (2011) 251–256.